Three-dimensional numerical simulation of the natural convection in an open tilted cubic cavity

J.F. Hinojosa[c], G. Alvarez[b], and C.A. Estrada[a]
[a]Centro de Investigación en Energía-UNAM,
Priv. Xochicalco s/n, Temixco, Morelos, Mexico,
Apartado Postal 34, 62580,
Tel. +52+55+56229729, Fax. +52+777+3250018.
e-mail: cestrada@cie.unam.mx
[b]CENIDET-SNIT-SEP,
Av. Palmira s/n. Col. Palmira, Cuernavaca, Morelos, Mexico
e-mail: gaby@cenidet.edu.mx
[c] Depto. de Ing. Química y Met., Universidad de Sonora,
Hermosillo, Sonora, Mexico
e-mail: fhinojosa@iq.uson.mx

In this work the numerical results of the heat transfer by natural convection in a tilted open cubic cavity are presented. The most important assumptions in the mathematical formulation are two: the flow is laminar, and the Boussinesq approximation is valid. The conservation equations in primitive variables are solved using the finite volume method and the SIMPLEC algorithm. The advective terms are approximated by the SMART scheme, and the diffusive terms are approximated using the central differencing scheme. The results in the steady state are obtained for a Rayleigh range from 10^4 to 10^7 and for a range of 0-180° for the inclination angles of the cavity. The results show that for high Rayleigh numbers, the Nusselt number changes substantially with the inclination angle of the cavity. The numerical model predicted Nusselt number oscillations for low angles and high Rayleigh numbers.

Keywords: Open cavities; natural convection; three dimensional numerical simulation.

En este artículo se presentan los resultados numéricos de transferencia de calor por convección natural en una cavidad cúbica abierta. En la formulación matemática las suposiciones más importantes son dos: el flujo es laminar y la aproximación de Boussinesq es válida. Las ecuaciones de conservación son presentadas en variables primitivas y son resultas usando el método de volumen finito y el algoritmo SIMPLER, los términos advectivos son aproximados por el esquema SMART y los difusivos por el esquema de diferencias centrado. Los resultados en estado permanente se presentan para números de Rayleigh en el rango 10^4 a 10^7, para ángulos de inclinación de la cavidad de 0 a 180°. Los resultados muestran que para números de Rayleigh altos, los números de Nusselt cambian sustancialmente con el ángulo de inclinación de la cavidad. Se encuentra que el modelo numérico predice oscilaciones del número de Nusselt para ángulos pequeños y números de Rayleigh altos.

Descriptores: Cavidades abiertas; convección natural; simulación numérica tridimensional.

PACS: 44.25.+f; 44.40.+a

1. Introduction

In solar concentrators, like a system of parabolic dish with a Stirling thermal engine, used to produce electricity, a tracking system rotates the solar concentrator, maintaining its optical axis pointing directly towards the sun. During the tracking, the geometry of the concentrator makes it possible to reflect the solar rays inside the receiver (open cavity) located at the focal point of the concentrator. The receiver, when rotated, will change the dynamic of the fluid and the heat transfer in the tilted open cavity. In order to have an accurate design for the it si important to study this process previously.

Over the past two decades, various numerical calculations and experimental results have been presented for describing the phenomena of natural convection in open cavities [1-16]. Those studies have focused on studying the effect on flow and heat transfer of different Rayleigh numbers, physical properties, aspect ratios and tilted angles. They, also studied the occurrence of transition and turbulence and the manner in which the boundary conditions in the aperture were considered.

However, only the paper of Sezai and Mohamad [12] presented three dimensional numerical results, of the natural convection in an open cavity with a fixed orientation (the heated vertical wall was opposite to the aperture while the remaining walls were adiabatic). The parametric study presented the variation of the flow pattern and heat transfer with respect to the Rayleigh number (10^3 to 10^6) and the lateral aspect ratios (2.0, 1.0, 0.5, 0.25 and 0.125). Comparing with two-dimensional results, the authors conclude that the two-dimensional results are valid for lateral aspect ratio equal to and greater than unity, and for Rayleigh numbers equal to and less than 1×10^5.

On the other hand, some papers have studied numerically the effect of the inclination angle of the cavity on the heat transfer and fluid flow [1,9,10,16], but they fail to cover the full range of inclination angles. The following is a summary of those papers.

Le Quere *et al.* [1] made a numerical study of two-dimensional natural convection in an isothermal open cav-

ity. The authors investigated the effect on the flow field and heat transfer of the Grashof number as it varied from 10^4 to 3×10^7; the temperature difference between the cavity walls and ambient changed from 50 to 500 K, the aspect ratio varied between 0.5 and 2, and the inclination angle of the cavity was modified from 0 to $45°$ (for $0°$ the wall opposite the aperture was vertical and the angles were taken clockwise). The results of the paper showed that the Nusselt number diminished with the increase in the inclination angle, and that the unsteadiness in the flow takes place for values of the Grashof number greater than 10^6 and inclination angles of $0°$.

Showole and Tarasuk [9] investigated, experimentally and numerically, the natural steady state convection in a two-dimensional isothermal open cavity. They obtained experimental results for air, varying the Rayleigh number from 10^4 to 5.5×10^5, cavity aspect ratios of 0.25, 0.5 and 1.0, and inclination angles of 0, 30, $45°$ and $60°$ (for $0°$, the wall opposite the aperture was horizontal and the angles were taken clockwise). The numerical results were calculated for Rayleigh numbers between 10^4 and 5.5×10^5, inclination angles of 0 and $45°$, and an aspect ratio equal to one. The results showed that, for all Rayleigh numbers, the first inclination of the cavity caused a significant increase in the average heat transfer rate, but a further increase in the inclination angle caused very little increase in the heat transfer rate. Another result observed was that, for $0°$, two symmetric counter rotating eddies were formed, while at inclination angles greater than $0°$, the symmetric flow and temperature patterns disappear.

Mohamad [10] studied numerically the natural convection in an inclined two-dimensional open cavity with one heated wall opposite the aperture and two adiabatic walls. The author analyzed the influence on fluid flow and heat transfer, with the inclination angle in the range $10°$-$90°$ (for $90°$ the wall opposite the aperture was vertical and the angles were taken clockwise), the Rayleigh number from 10^3 to 10^7, and the aspect ratio between 0.5 and 2. The study concludes that the inclination angle did not have a significant effect on the average Nusselt number from the isothermal wall, but a substantial one on the local Nusselt number.

Polat and Bilgen [16] made a numerical study of the conjugate heat transfer by conduction and natural convection in an inclined, open shallow cavity with a uniform heat flux in the wall opposite to the aperture. The parameters studied were: the Rayleigh number from 10^6 to 10^{12}, the conductivity ratio from 1 to 60, the cavity aspect ratio from 1 to 0.125, the dimensionless wall thickness from 0.05 to 0.20, and the inclination angle from 0 to $45°$ from the horizontal (for $0°$, the wall opposite the aperture was vertical and the angles were taken counterclockwise). The authors found that at high Rayleigh numbers, the volume flow rate is a decreasing function of the inclination angle of the cavity, while the heat transfer is an increasing function of it. At low Rayleigh numbers, the functional relationship is reversed.

In the present paper, a numerical study of natural convection in an open cubic cavity, varying the Rayleigh number through the range of 10^4 to 10^7 and changing the inclination angle from 0 to $180°$. This study is an effort to obtain more accurate heat transfer and fluid flow results in open tilted cavities.

2. Description of the physical problem

The heat transfer and the fluid flow in a three dimensional open tilted cubic cavity of length L, was considered in the present investigation as shown in Fig. 1. The wall opposite to the aperture was kept at a constant temperature T_H, while the surrounding fluid interacting with the aperture was at ambient temperature T_∞; which was lower than T_H, the four remaining walls were assumed adiabatic. The thermal fluid was assumed to be air (Pr=0.71), and it was considered laminar and Newtonian. The properties of the fluid were assumed to be constant except for the density in the buoyant force term in the momentum equations, according to the Boussinesq approximation.

3. Governing equations and boundary conditions

The transient state dimensionless conservation equations governing the transport of mass, momentum and energy in primitive variables are expressed as

Continuity

$$\frac{\partial U}{\partial X} + \frac{\partial V}{\partial Y} + \frac{\partial W}{\partial Z} = 0 \qquad (1)$$

X-momentum

$$\frac{\partial U}{\partial \tau} + \frac{\partial (U^2)}{\partial X} + \frac{\partial (VU)}{\partial Y} + \frac{\partial (WU)}{\partial Z} = -\frac{\partial P}{\partial X}$$
$$+ \left(\frac{\mathrm{Pr}}{Ra}\right)^{1/2} \left(\frac{\partial^2 U}{\partial X^2} + \frac{\partial^2 U}{\partial Y^2} + \frac{\partial^2 U}{\partial Z^2}\right) + \theta \cos\phi \quad (2)$$
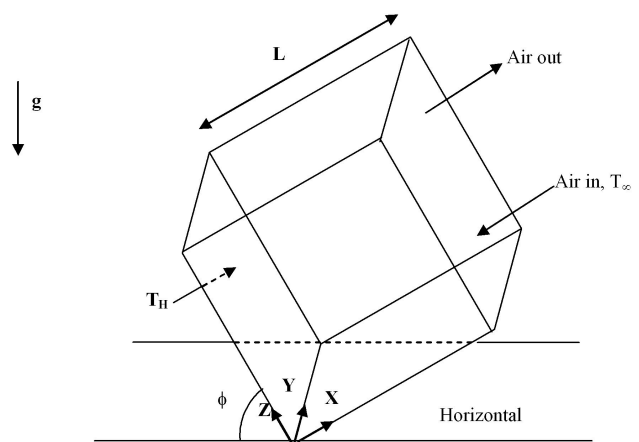

FIGURE 1. Scheme of the open tilted cubic cavity.

Y-momentum

$$\frac{\partial V}{\partial \tau} + \frac{\partial (UV)}{\partial X} + \frac{\partial (V^2)}{\partial Y} + \frac{\partial (WV)}{\partial Z} = -\frac{\partial P}{\partial Y}$$
$$+ \left(\frac{Pr}{Ra}\right)^{1/2} \left(\frac{\partial^2 V}{\partial X^2} + \frac{\partial^2 V}{\partial Y^2} + \frac{\partial^2 V}{\partial Z^2}\right) \quad (3)$$

Z-momentum

$$\frac{\partial W}{\partial \tau} + \frac{\partial (UW)}{\partial X} + \frac{\partial (VW)}{\partial Y} + \frac{\partial (W^2)}{\partial Z} = -\frac{\partial P}{\partial Z}$$
$$+ \left(\frac{Pr}{Ra}\right)^{1/2} \left(\frac{\partial^2 W}{\partial X^2} + \frac{\partial^2 W}{\partial Y^2} + \frac{\partial^2 W}{\partial Z^2}\right) + \theta \sin \phi \quad (4)$$

energy

$$\frac{\partial \theta}{\partial \tau} + \frac{\partial (U\theta)}{\partial X} + \frac{\partial (V\theta)}{\partial Y} + \frac{\partial (W\theta)}{\partial Z} = \frac{1}{(Pr\, Ra)^{1/2}}$$
$$\times \left(\frac{\partial^2 \theta}{\partial X^2} + \frac{\partial^2 \theta}{\partial Y^2} + \frac{\partial^2 \theta}{\partial Z^2}\right) \quad (5)$$

where $Ra = [g\beta L^3 (T_H - T_\infty)]/\alpha\nu$ is the Rayleigh number, and $Pr = \nu/\alpha$ is the Prandtl number.

The above equations were non-dimensionalized by defining

$$X = x/L, \quad Y = y/L, \quad Z = z/L,$$
$$\tau = U_o t/L, \quad P = \frac{p - p_\infty}{\rho U_o^2} \quad U = u/U_o,$$
$$V = v/U_o, \quad W = w/U_o, \quad \theta = \frac{T - T_\infty}{T_H - T_\infty}. \quad (6)$$

The reference velocity U_o is related to the buoyancy force term and it is defined by $U_0 = [g\beta L(T_H - T_\infty)]^{1/2}$ [6].

The initial and boundary conditions for the momentum and energy equations were similar to the ones used by Chan and Tien [4] and Mohamad [10]. An important characteristic of those boundary conditions is the use of an approximation in the aperture plane, which allows us to truncate the computational domain and to reduce the computational time. At the opening, the temperature of the incoming fluid was fixed at the ambient temperature, while for the outgoing fluid the temperature gradient was zero. This is due to the assumption that thermal conduction is negligible compared to the value of the thermal convection; therefore, the isotherms were normal to the aperture. For the momentum equations, the zero-gradient condition was also used, and then the velocity components were in a direction normal to the opening. The initial and boundary conditions were taken as follows:

Initial conditions

$$P(X, Y, 0) = U(X, Y, 0) = V(X, Y, 0) = W(X, Y, 0)$$
$$= \theta(X, Y, 0) = 0 \quad (7)$$

Momentum boundary conditions

$$U(0, Y, Z, \tau) = U(X, 0, Z, \tau) = U(X, 1, Z, \tau)$$
$$= U(X, Y, 0, \tau) = U(X, Y, 1, \tau) = 0$$
$$V(0, Y, Z, \tau) = V(X, 0, Z, \tau) = V(X, 1, Z, \tau)$$
$$= V(X, Y, 0, \tau) = V(X, Y, 1, \tau) = 0$$
$$W(0, Y, Z, \tau) = W(X, 0, Z, \tau) = W(X, 1, Z, \tau)$$
$$= W(X, Y, 0, \tau) = W(X, Y, 1, \tau) = 0$$
$$\left(\frac{\partial U}{\partial X}\right)_{X=1} = \left(\frac{\partial V}{\partial X}\right)_{X=1} = \left(\frac{\partial W}{\partial X}\right)_{X=1} = 0 \quad (8)$$

Energy boundary conditions

$$\theta(0, Y, \tau) = 1$$
$$\theta \left(\frac{\partial \theta}{\partial Y}\right)_{Y=0} = \left(\frac{\partial \theta}{\partial Y}\right)_{Y=1} = \left(\frac{\partial \theta}{\partial Z}\right)_{Z=0}$$
$$= \left(\frac{\partial \theta}{\partial Z}\right)_{Z=1} = 0 \quad (9)$$

The local convective Nusselt number can be obtained from the temperature field by applying

$$Nu = -\left(\frac{\partial \theta(Y, Z)}{\partial X}\right)_{X=0}. \quad (10)$$

The average convective Nusselt number was calculated by integrating the temperature gradient over the heated wall as

$$\overline{Nu} = -\int_0^1 \int_0^1 \left(\frac{\partial \theta}{\partial X}\right) dY\, dZ \quad (11)$$

4. Numerical method of solution

Equations (1)-(5) were discretized using staggered, uniform control volumes. The convective terms were approximated by the SMART scheme [17] and the diffusive terms with the central differencing scheme. The SIMPLEC algorithm [18] was used to couple continuity and momentum equations. The fully implicit scheme was used for the time discretization. The resulting system of linear algebraic equations was solved iteratively by the SIP method [19].

A grid independent solution is ensured by comparing the result of different grid meshes for $Ra = 1 \times 10^7$, which was the highest Rayleigh number. Figure 2 show the history of the average Nusselt number for grid sizes of $50 \times 50 \times 50$, $60 \times 60 \times 60$, $70 \times 70 \times 70$ and $80 \times 80 \times 80$. This figure presented the dependent time average Nusselt numbers because for $Ra = 1 \times 10^7$, the steady state cannot be reached. The difference between predictions of $70 \times 70 \times 70$ and $80 \times 80 \times 80$ is less than 1.0%, and then the calculations were obtained with the $70 \times 70 \times 70$ grid mesh. The dimensionless time step used for the calculations was 1×10^{-3}.

TABLE I. Comparison between the average Nusselt numbers calculated in the present 3-D model with those of the 2-D model reported in [10] and those reported from Sezai and Mohammad [12].

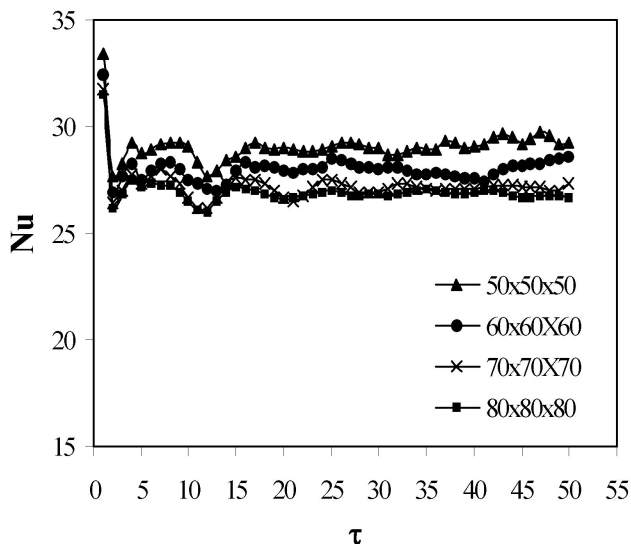| ϕ	10^4	10^5	10^6	10^7
			Ra	
		3D model (this work)		
10°	3.25	10.11±0.24	18.5±1.58	——
30°	3.56	7.78	14.52	29.64±5.08
60°	3.71	7.51	14.05	28.1±0.2
90°	3.38	7.32	14.35	27.2±0.3
		2D model [10]		
10°	2.57	6.87	16.21	——
30°	3.34	6.17	12.08	27.3±5.0
60°	3.7	7.36	13.72	29.2±5.0
90°	3.44	7.41	14.36	28.6±2.5
		3D model [12]		
90°	2.864	6.872	13.961	——

FIGURE 2. Grid independence test: (a) Local convective Nusselt numbers along the heated wall, (b) U-velocity at the aperture for different grid size.

5. Results

Results are presented for natural convection for open, tilted cavities in the range of Ra of 10^4-10^7, and inclination angles of 0, 45, 90, 135 and 180°. In order to investigate the effect of three dimensionality over 2-D, for the tilted angles of 10, 30, 60 and 90°, and verify the computer code, Table I presents the comparison of the 3-D present results with those reported in the literature for 2-D and 3-D [10,12]. The percentage differences between 3D model (this study) and 2D model [10] were in the range 0.3-20.6%. As the tilted angle decreases, the difference between the 2-D and 3-D results becomes significant,

showing the effect of three dimensionality on the open cavity. To verify the computer code, we compare the present 3-D results for 90° with those reported from Sezai and Mohammad [12]: the average Nusselt number percentage differences are in the range of 2.6-15.1%, with an average value of 8 %. The highest difference corresponds to Ra=10^4, with the lowest Nusselt number. Because the percentage differences are relatively high, we modify our computer code, changing the boundary conditions from the open cavity to a closed cavity as a strategy to have a more detailed verification of the computer code against the benchmark results of Wakashima and Saitoh [20], which they considered a classical problem of a closed cavity with hot and cold vertical isothermal walls. From this comparison, we obtained an average percentage difference of less than 1% for the average Nusselt number, so we considered the computer code sufficiently tested.

In Fig. 3, the isotherm behavior for a range of Ra of 10^4-10^7 and inclination angles of 0, 45, 90, 135, and 180° in the plane Y=0.5, are shown. We observed that, for ϕ =0°, the hot fluid enters by the center of the cavity and leaves near the vertical adiabatic walls, except for Ra=10^4, where the cold fluid enters close to the right adiabatic wall of the cavity, while the hot fluid leaves the cavity close to the left adiabatic wall. Several thermal plumes were observed in the bottom hot wall and along the vertical adiabatic walls for ϕ=0° and Rayleigh numbers of 10^6 and 10^7. It should be noted that this case is similar to the Rayleigh-Benard problem, but without the upper rigid boundary. When the Rayleigh number increases above a critical value, the temperature gradient (buoyant force) exceeds the dissipative effects of the viscous drag and heat diffusion, causing an ascending fluid motion. For high Rayleigh numbers, the magnitude of the buoyant force causes the fluid to rise quickly, forming thermal plumes to emerge from the bottom heated wall, forming an unsteady convection and causing fluctuations in the Nusselt number.

When the cavity was tilted to 45°, the cold fluid penetration was from the right bottom part of the adiabatic wall. The thickness of the boundary layer of the hot wall decreases as the Rayleigh number increases. For the case of ϕ=90°, the isotherm pattern was similar to those observed in ϕ=45°; the thermal boundary layers from the hot vertical wall and the top adiabatic wall become thinner as the Rayleigh number increases. The thermal gradients of the thermal boundary layer at the top wall for Ra = 10^7 increases. But when the tilted angle was 135°, the isotherms indicate a decrease in the heat transfer rate compared with ϕ=90°. For this 135° angle, a stratification zone shown by the horizontal isothermal lines begins to appear at the middle of the tilted cavity. Finally, when Ra=10^4, the cavity rotates 180°, the isotherm pattern indicates that conduction dominates the heat transfer process.

In order to show the basic flow pattern characteristics at the entrance to the cavity, the profiles of the U-velocity in the aperture plane (X=1) for Ra=10^4 and inclination angles of 0, 45, 90, 135 and 180°, are presented in Fig. 4. For a cavity
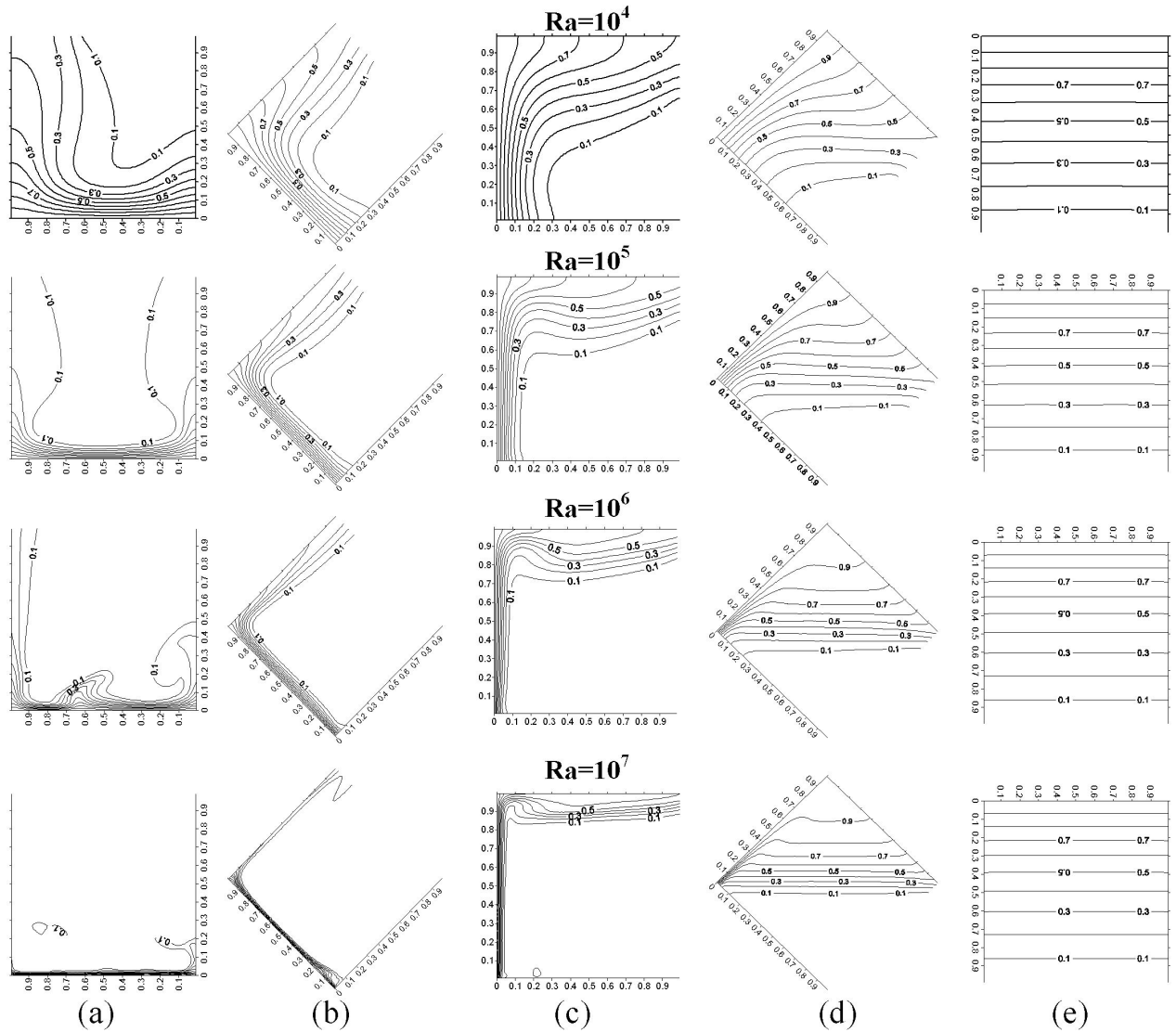
FIGURE 3. Isotherms in the plane Y=0.5, for different values of the Rayleigh number and some values of the inclination angle: (a) 0°, (b) 45°, (c) 90°, (d) 135°, and (e) 180°.

with ϕ=0°, the fluid enters and leaves, obliquely with respect to the coordinate axis, the dimensionless magnitudes of the U-velocity of the airflow go from –0.3 to 0.6 meaning that the air comes in slowly and leaves quickly. It should be noted that, due to the fact that the symmetry of the problem multiple solutions exists, for example if the sign of the U-velocity is changed, another solution is obtained and then a more detailed study must be done of this specific orientation. When the angle of the cavity increases from 45 to 90°, the U-velocity of the cold fluid entering becomes slower and that of the air leaving becomes faster, but the cross sectional area occupied by the leaving air decreases. Thus the boundary layer at the top of the aperture plane becomes thinner. For the tilted angle of 135°, the air leaving the top of the cavity decreases its U-velocity to 0.2. Finally, when the aperture of the cavity is facing downward (180°), the fluid practically does not cross the aperture, indicating stagnation in the air flow.

Figure 5 presents the W-velocity profiles in the plane Z=0.5, for Ra=10⁴ and inclination angles of the cavity of 0, 45, 90, 135 and 180°. A thinner hydrodynamic boundary layer can be observed for inclination angles of the cavity between 45 and 90°, with none vertical movement in the central section of the cavity. The basic flow pattern for those angles is that the fluid enters from the inferior side of the aperture, circulates clockwise following the shape of the cavity, and leaves towards the upper side of the aperture. At ϕ=0°, the dimensionless W-velocity is slightly above 0.12, then increases for ϕ=45° and 90° up to 0.27. When the cavity rotates to an angle of 135°, two vertical W-velocity displacements of the fluid can be observed. The first one next to the hot wall, induced by the buoyancy force, reaches the value of 0.10. The second vertical movement corresponds to the hot fluid leaving in a obliquely with a W-velocity component of 0.04. Finally, when the cavity is at an angle of 180°, the fluid W-velocity becomes zero, indicating that the air stands still.

FIGURE 4. Velocity-U profiles in the aperture plane (X=1) for Ra=10^4 and some inclination angles of the open cavity.

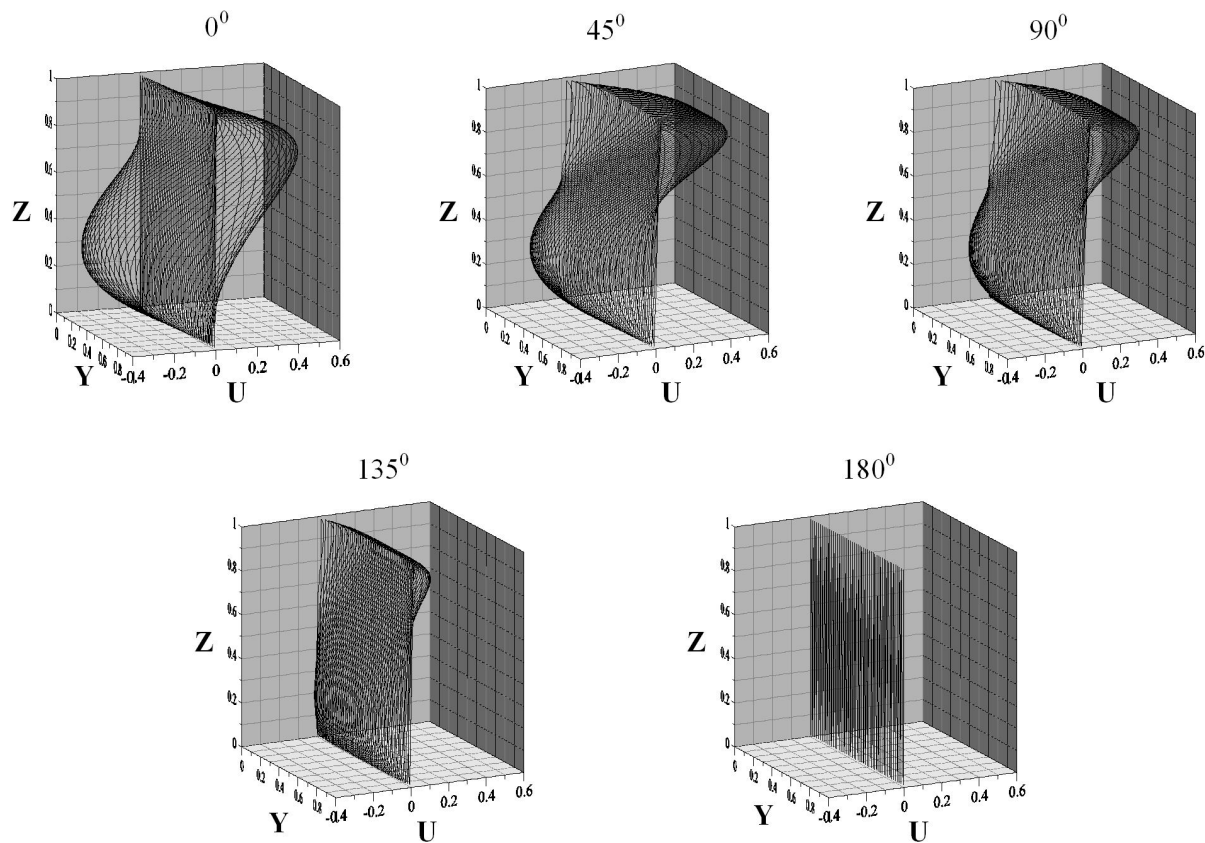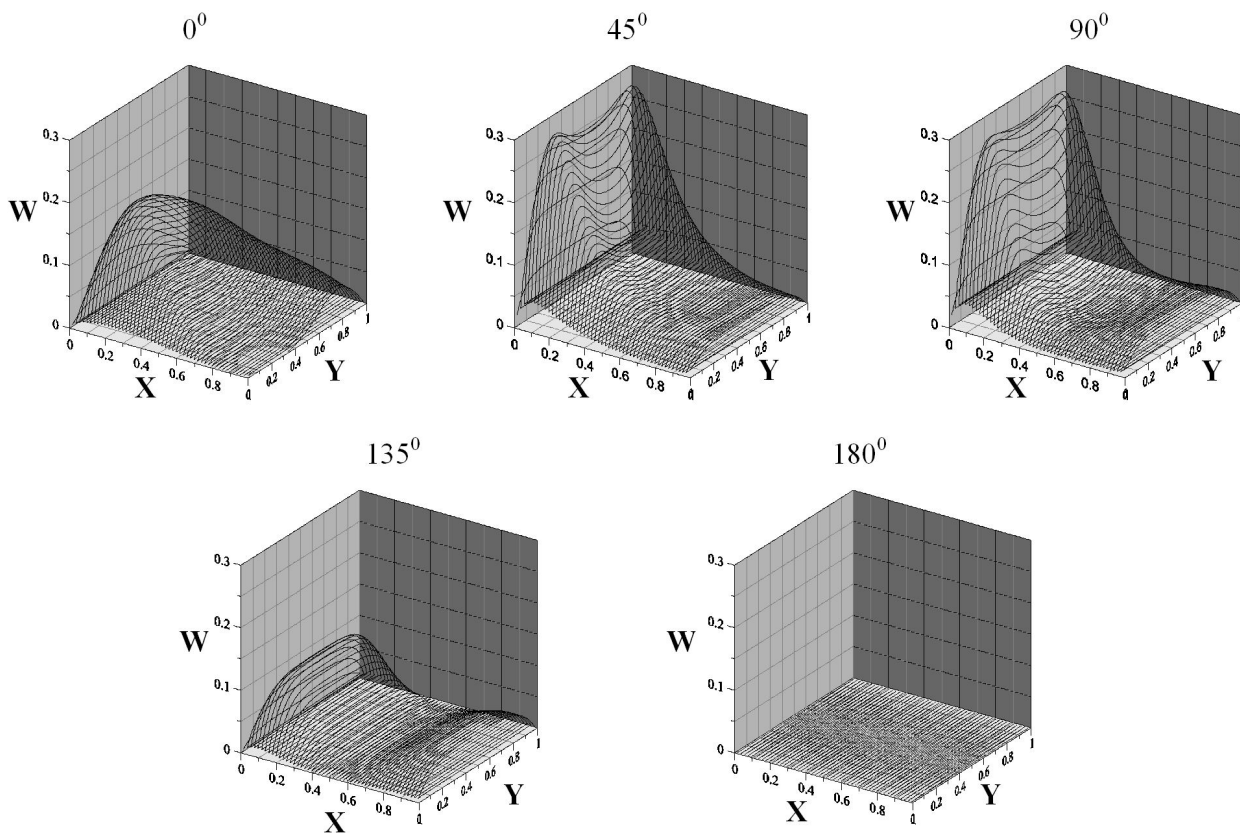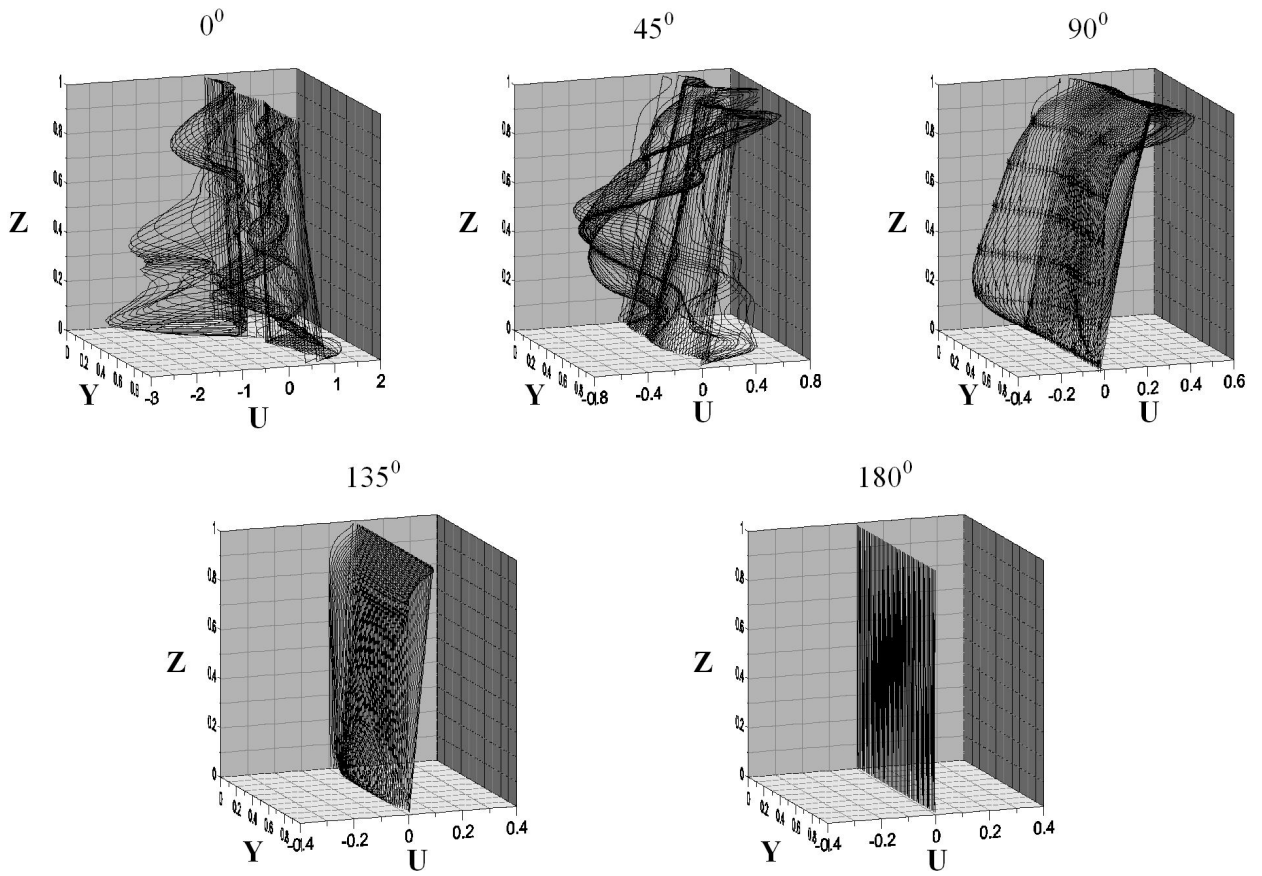FIGURE 5. W-velocity profiles in the plane (Z=0.5) for Ra=10^4 and some inclination angles of the open cavity.

FIGURE 6. Velocity-U profiles in the aperture plane (X=1) for Ra=10^7 and some inclination angles of the open cavity.
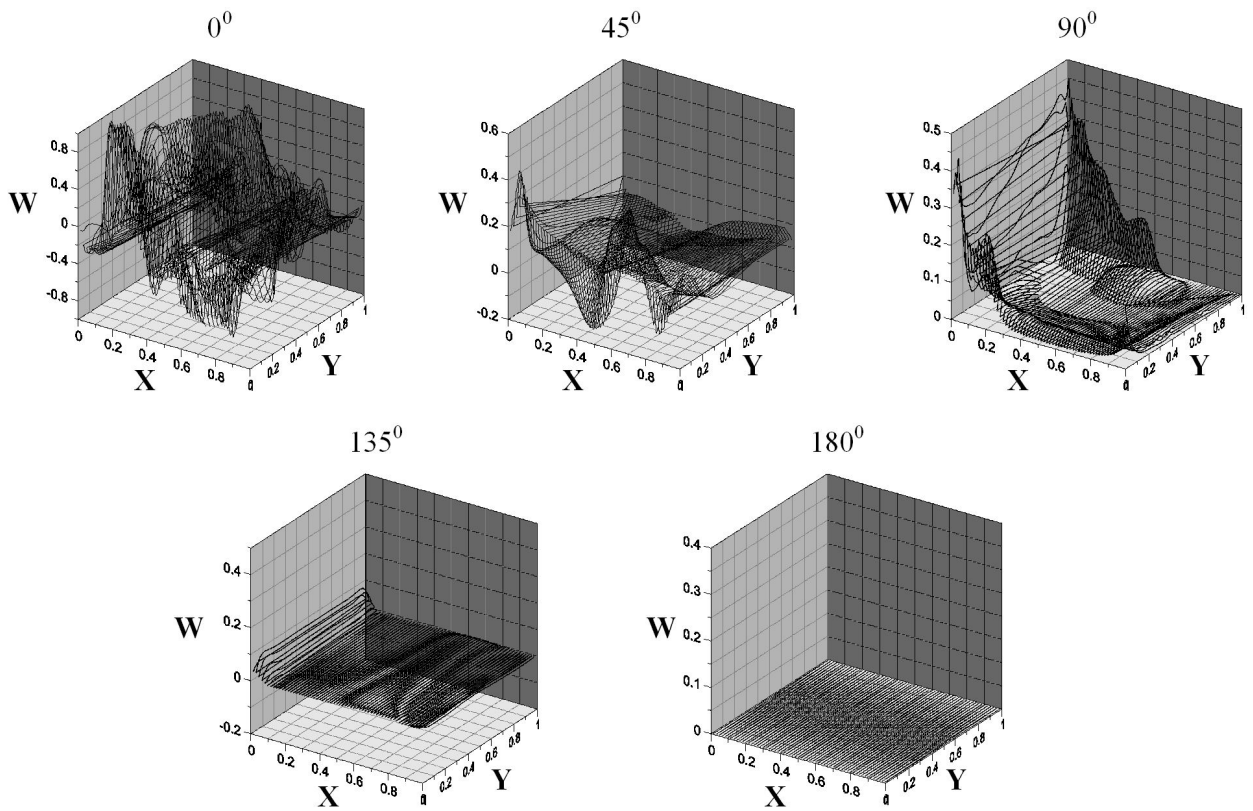

FIGURE 7. W-velocity profiles in the plane (Z=0.5) for Ra=10^7 and some inclination angles of the open cavity.

TABLE II. Average Nusselt numbers for different cavity's inclination angles and Rayleigh numbers, obtained with de 3D model.

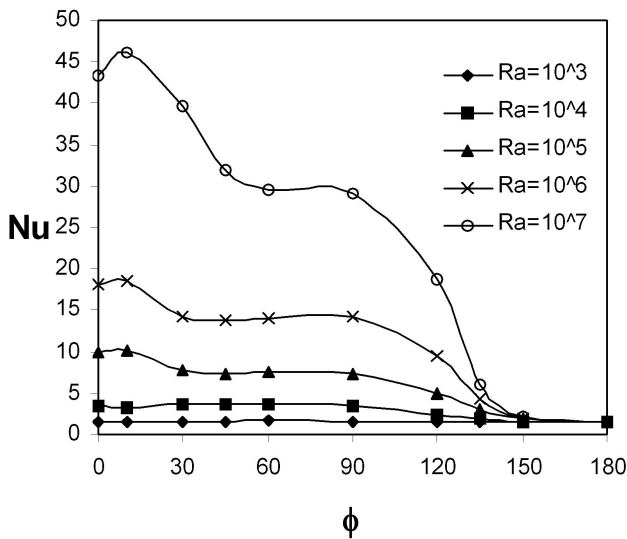| ϕ	10^4	10^5	10^6	10^7
			Ra	
0°	3.45	9.96±0.06	18.18±1.14	41.27±11.23
10°	3.25	10.11±0.24	18.48±1.43	44.2±6.83
30°	3.56	7.78	14.33±0.09	37.64±5.08
45°	3.69	7.37	13.81	30±3.08
60°	3.71	7.51	14.05	28.1±0.91
90°	3.38	7.32	14.33	27.21±0.74
120°	2.43	4.90	9.55	18.67
135°	1.93	2.96	4.32	6.05
150°	1.59	1.85	1.86	2.08
180°	1.44	1.45	1.45	1.45

FIGURE 8. Average Nusselt number as a function of the inclination angle of the cavity for five Rayleigh numbers.

With the increase of the Rayleigh number, complex flow pattern characteristics were found for some inclination angles. To show this, the profiles of the U-velocity in the aperture plane (X=1) for Ra=10^7 and inclination angles of 0, 45, 90, 135 and 180°, are presented in Fig. 6. For angles of the cavity between 0 and 45°, the steady state can not be reached; the instantaneous pictures show that the fluid enters and leaves in a very irregular way, indicating an unsteady convection. When the cavity angle increases to 90°, the air flow again can not reach the steady state, but the flow pattern is more regular. The cold fluid enters by the lower section of the aperture plane, without symmetry, and the hot fluid leaves by the upper section. The U-velocity magnitude of the leaving fluid is greater than the incoming fluid, and thus the hydrodynamic boundary layer at the top wall becomes much thinner. For the tilted angle of 135°, the air flow entering and leaving the cavity decreases its U-velocity considerably.

Finally, when the aperture of the cavity is facing downward (180°), the fluid practically does not cross the aperture, indicating that that air is stagnant.

In order to complete the previous description of the fluid flow patterns for Ra=10^7, Fig. 7 presents the W-velocity profiles for the cross sectional plane Z=0.5, and the inclination angles of the cavity of 0, 45, 90, 135 and 180°. An irregular ascending and descending flow can be observed for inclination angles of the cavity between 0 and 45°. At ϕ=90°, a thin hydrodynamic boundary layer can be observed adjacent to the heated wall, with ascending fluid near the lateral adiabatic walls. When the cavity rotates to the angle of 135°, a slow vertical W-velocity movement of the fluid can be observed adjacent to the hot wall, induced by the buoyancy force with a value of 0.10. Finally when the cavity has an inclination angle of 180°, the fluid W-velocity becomes zero, indicating that the air is stagnant.

Table II presents the average Nusselt numbers for four Rayleigh numbers (10^4, 10^5, 10^6 and 10^7) for a range of 0-180° for the tilted angles of the open cavity. For different angles and Ra numbers, mainly for lower angles and higher Ra, the average Nusselt number oscillates periodically and the steady state is not reached. Therefore, in Table II, the average Nusselt numbers and their standard deviation are reported.

In Fig. 8 the results of Table II are presented in order to show the effect of the Rayleigh number and the inclination angle of the cavity (the average Nu was considered when oscillations were observed). The figure shows that the average Nusselt number, for a fixed Rayleigh number, changes notably with respect to the cavity's inclination angle. For angles within the range 0-90° and Ra number from 10^4-10^6, the Nu number remains approximately constant, while for angles higher than 90°, it decreases. For Ra=10^7, the Nusselt number begins high at 0° and increases at 10°, but then decreases at 30° and 45°, but at 60 and 90° remains similar and afterwards decreases. For all the Rayleigh numbers the minimum average Nusselt number corresponds to 180°.

Finally, a set of correlations for the average Nusselt numbers for the steady state (again the average Nu was used for the cases where oscillations were detected) were obtained using a least-square regression technique for $10^4 \leq Ra \leq 10^7$, namely:

$$Nu = \exp(-1.736 + -0.0053\phi + 0.34\ln(Ra))$$
$$\text{for} \quad 0° \leq \phi \leq 90°$$
$$Nu = (-1.29 + 0.008\phi + 5.53/\ln(Ra))^{-1}$$
$$\text{for} \quad 120° \leq \phi \leq 180° \quad (12)$$

A pair of correlation equations was necessary, because of the complexity of the Nusselt number distribution and to keep the equations as simple as possible.

6.   Conclusions

In this paper, the steady state numerical calculations of natural convection in a tilted open cavity were presented. The main conclusions of this work were the following:

1. The average Nusselt number changed substantially with the inclination angle of the cavity.

2. The inclination angles in the range of $0°$–$90°$ of the cavity increase the heat transfer, because they facilitated the exit of the heated fluid.

3. The inclination angles between $120°$ and $180°$ of the cavity decrease the heat transfer, because they obstruct the exit of the heated fluid.

4. Instabilities in the air flow, and oscillations in the average Nusselt number for low angles and high Rayleigh numbers (10^5 - 10^7), were observed.

Acknowledgment

Appendix

Notation

g	gravitational acceleration,	m/s^2	U$_o$	reference convective velocity,	m/s
k	thermal conductivity,	W/m-K	u,v,w	velocity components,	m/s
L	length of the cavity,	m	U,V,W	dimensionless velocity components	
Nu	local Nusselt number		x,y,z	coordinate system,	m
$\overline{Nu}$	average Nusselt number		X,Y,Z	dimensionless coordinates	
P	pressure,	N/m^2			
P	dimensionless pressure,	$p\text{-}p_\infty/\rho u_\infty^2$	***Greek letter***		
Pr	Prandtl number,	$[=\nu/\alpha]$	α	thermal diffusivity,	m^2/s
Ra	Rayleigh number		β	thermal expansion coefficient,	1/K
T	absolute temperature,	K	ϕ	inclination angle of the cavity,	degrees
T$_H$	temperature of the heated wall,	K	ν	kinematic viscosity,	m^2/s
T$_\infty$	temperature of the environment,	K	θ	dimensionless temperature	
t	time,	s	τ	dimensionless time	

1. P. Le Quere, J.A. Humphrey, and F.S. Sherman, *Numerical Heat Transfer* **4** (1981) 249.

2. F. Penot, *Numerical Heat Transfer* **5** (1982) 421.

3. Y.L. Chan and C.L. Tien, *Numerical Heat Transfer* **8** (1985) 65.

4. Y.L. Chan and C.L. Tien, *International Journal of Heat and Mass Transfer* **28** (1985) 603.

5. Y.L. Chan and C.L. Tien, *Journal of Heat Transfer* **108** (1986) 305.

6. J.A.C. Humphrey and W.M. To, *International Journal of Heat and Mass Transfer* **29** (1986) 593.

7. K. Vafai and J. Ettefagh, *International Journal of Heat and Mass Transfer* **33** (1990) 2311.

8. D. Angirasa, M.J. Pourquié, and F.T. Nieuwstadt, *Numerical Heat Transfer Part A* **22** (1992) 223.

9. R.A. Showole and J.D. Tarasuk, *Journal of Heat Transfer* **115** (1993) 592.

10. A.A. Mohamad, *Numerical Heat Transfer Part A* **27** (1995) 705.

11. W. Chakroun, M.M. Elsayed, and S.F. Al-Fahed, *Journal of Solar Energy Engineering* **119** (1997) 298.

12. I. Sezai and A.A. Mohamad, *International Journal of Numerical Methods for Heat and Fluid Flow* **8** (1998) 800.

13. M.M. Elsayed and W. Chakroun, *Journal of Heat Transfer* **121** (1999) 819.

14. K. Khanafer and K. Vafai, *International Journal of Heat and Mass Transfer* **43** (2000) 4087.

15. K. Khanafer and K. Vafai, *International Journal of Heat and Mass Transfer* **45** (2002) 2527.

16. O. Polat and E. Bilgen, *International Journal of Heat and Mass Transfer* **46** (2003) 1563.

17. P.H. Gaskell and A.K.C. Lau, *International Journal of Numerical Methods in Fluids* **8** (1988) 617.

18. J.P. Van Doormaal and G.D. Raithby, *Numerical Heat Transfer* **7** (198)4 147.

19. H.L. Stone, *Journal of Numerical Analysis* **5** (1968) 530.

20. S. Wakashima and T.S. Saitoh, *International Journal of Heat and Mass Transfer.* **47** (2004) 853.